Superconductor Science and Technology

Critical current anisotropy of GdBCO tapes grown on ISD–MgO buffered substrate

IOP Publishing Superconductor Science and Technology
Supercond. Sci. Technol. **28** (2015) 124002 (8pp) doi:10.1088/0953-2048/28/12/124002

Critical current anisotropy of GdBCO tapes grown on ISD–MgO buffered substrate

M Lao[1], J Bernardi[2], M Bauer[3] and M Eisterer[1]

[1] Atominstitut, TU Wien, Stadionallee 2, 1020, Vienna, Austria
[2] University Service Center for TEM, TU Wien, Wiedner Hauptstrasse 8-10, 1040, Vienna, Austria
[3] THEVA Duennschichttechnik GmBH, Rote-Kreuz Strasse 8, D-85737, Ismaning, Germany

E-mail: mlao@ati.ac.at

Received 16 July 2015, revised 15 September 2015
Accepted for publication 23 September 2015
Published 23 October 2015

Abstract

The critical current anisotropy of a $GdBa_2Cu_3O_7$ (GdBCO) coated conductor (CC) was investigated. The MgO buffer layer was grown by the inclined substrate deposition (ISD) technique leading to a tilted *c*-axis growth of the GdBCO layer by 24° from the tape normal. The J_c was measured in two current directions: longitudinal and transverse to the tape. The self-field J_c in the 2 μm thick GdBCO layer was 1.3 MA cm^{-2} and 0.88 MA cm^{-2} at 77 K in the longitudinal and transverse directions, respectively. The 30% lower value in the transverse direction results from the current flow across the weakly superconducting layer of GdBCO. The peak in the J_c-anisotropy corresponding to intrinsic pinning appears at 24° with respect to the tape surface in the longitudinal direction and the anisotropy was highly asymmetric in a wide range of fields. Due to the large crystallographic tilt of the GdBCO with respect to the tape axes, a minimum caused by vortex channeling occurred in the transverse current direction which was observed for the first time at 77 K. Another consequence of the large crystallographic tilt angle is a pronounced competing effect of the crystallographic anisotropy and Lorentz force on J_c in the variable Lorentz force configuration.

Keywords: coated conductors, critical currents, anisotropy, GdBCO, ISD, vortex channeling

1. Introduction

One of the biggest challenges in (RE)$Ba_2Cu_3O_{7-\delta}$ (REBCO, RE = rare Earth metal) coated conductor fabrication is the strong degradation of the critical current density, J_c, with increasing thickness of the superconducting layer. Various studies find that the increase in thickness leads to the formation of cracks, voids, misorientation, impurities and other phases that block current flow [1–3]. A promising method to overcome this problem is the use of substrates made by the inclined substrate deposition (ISD) technique. THEVA GmbH has been producing REBCO CCs using the ISD method and finds an almost linear increase in I_c up to a thickness of 7.5μm. One benchmark value is a self-field I_c of 1018 A cm^{-1} at 77 K for a 5.9 μm thick $DyBa_2Cu_3O_{7-\delta}$ (DyBCO) CC [4]. The DyBCO grains in the tapes have a high biaxial texture because their inclined orientation suppresses *a*-axis growth. With these characteristics of the superconducting layer, Aabdin *et al* reported that J_c does not decrease significantly with increasing thickness and that J_c of a 6 μm DyBCO is very close to that of a 1 μm thick tape [5]. The superconducting layer has tilted crystallographic axes with respect to the tape surface and tilted and faceted grain boundaries [4]. The tilt of the grain boundaries with respect to the substrate normal in these CCs is 20–40° [5]. Due to the tilted crystallographic orientation in CCs produced on ISD templates, one can already deduce a reduced symmetry in the J_c anisotropy compared to conventional tapes with *ab*-planes parallel to the tape surface. The characteristic of the ISD CC renders it a very interesting material for the study of vortex physics.

The pinning of vortices is an essential element that directly affects the critical current density. A large variety of REBCO coated conductor architecture utilizes different material defects to optimize the pinning landscape that leads to a high J_c and a decrease of its anisotropy. The most common method is introducing secondary phases that form correlated defects aligned in a specific orientation through the

layer thickness [1, 6]. Aside from pinning by the engineered correlated defects, the J_c-anisotropy is also influenced by different factors inherent to the material such as intrinsic pinning by the layered crystal structure of cuprates [7], surface barrier [8] and sample geometry [9]. The influence of those features is stronger in superconducting films and tapes with reduced symmetry, such as films deposited on miscut substrates and ISD tapes.

In a layered superconductor, vortices are predicted to undergo a transition from an Abrikosov rectilinear vortex state to a kinked vortex state when the applied field $\vec{H}$ is rotated by an angle Θ with respect to the layers. The angular range where the kinked state occurs depends on the lattice spacing d of a superconductor, the Ginzburg–Landau coherence length ξ_{ab} along the *ab*-planes and the anisotopy parameter ε. The kinked state of a superconductor is composed of a stack of pancake vortices connected by Josephson strings. A fully formed kinked state is predicted to form within an angular regime of $\Theta < \tan^{-1}\varepsilon$. The transition to the kinked state occurs within $\tan^{-1}\varepsilon < \Theta < \tan^{-1}(d/\xi_{ab})$ and Abrikosov rectilinear vortices form at $\Theta > \tan^{-1}(d/\xi_{ab})$ [10].

The dynamics of the kinked vortex structure can be investigated in samples with reduced symmetry which allows a configuration where the Lorentz force is parallel to a planar defect. These planar defects can be the weakly superconducting planes of cuprates and grain boundaries. Since the vortex string segments are subjected to weaker pinning than the pancake vortices, a particular feature in the J_c-anisotropy, known as vortex channeling, is observed. It manifests as a strong and local decrease of J_c in its angular dependence when the Lorentz force drives cross-cutting and motion of the vortex strings along the planar defects. This effect has been reported in various materials such as vicinal YBCO films [11, 12], MOCVD/IBAD CCs [13] and samples with planar grain boundaries [14, 15] and twin boundaries [16].

In this paper, a $GdBa_2Cu_3O_{7-\delta}$ (GdBCO) coated conductor was produced on an ISD–MgO buffered substrate with the same architecture and deposition technique as the large-current DyBCO CC [4]. Information on the angular dependence of J_c for this high-potential GdBCO tape architecture is very important not just for cable design and magnet applications but to foster an understanding of vortex dynamics and its impact on industrial grade materials with tilted crystallographic axes.

2. Experimental procedure

The coated conductor used in this study has a 2 μm thick GdBCO superconductor layer deposited by co-evaporation on an ISD-grown MgO buffer layer on Hastelloy C-276. Details on the deposition process for CCs produced by this method are discussed elsewhere [17]. Due to the interesting geometry of the tilted crystallographic axes of this tape, two configurations of bridges were patterned from the GdBCO tape. The first one was parallel to the longitudinal direction of the tape in which the current flows along the *ab*-planes as shown by the red arrow in figure 1(a). It will be referred to as the L-bridge. The second was in the transverse direction, called the T-bridge, in which the current crosses the *ab*-planes. Wet chemical etching was performed to narrow the width of the bridges down to 350 μm for the L-bridge and 180 μm for the T-bridge.

The transport J_c-anisotropy was measured by using the four probe method with a voltage criterion of 2 μV cm^{-1}. Two measurement configurations were applied. The first one was under maximum Lorentz force (MLF) in which the direction of the applied magnetic field was maintained to be perpendicular to the current direction. By convention of our experimental set-up, this was achieved when the sample was rotated only about an axis parallel to the current flow. The corresponding angle is denoted by ϕ in figure 1(b). The angular orientation of the magnetic field with respect to the sample was checked with a precision of 0.5° using a Hall probe attached to the sample rod. The variable Lorentz force (VLF) configuration was established by using a two-axis goniometer sample rod, which enabled an additional rotation about an axis perpendicular to the current direction, represented by the angle θ in figure 1(b). The rotation in θ was calibrated with a Hall probe prior to the measurement and the rotation had a precision of about 1°. As a convention, when θ was rotated to 90°, the scan about the angle ϕ was called in-plane (IP) measurement because the applied field remains parallel to the plane of the tape. All the J_c-transport measurements were done in a helium gas flow cryostat with a split-coil superconducting magnet that can generate magnetic fields up to 5.5 T. The temperature can be stabilized between 4.2 K and 330 K. The transport J_c was measured at temperatures down to 20 K in the MLF configuration but measurements were restricted to temperatures above 60 K in the VLF configuration due to the maximum current of the two-axis goniometer sample rod.

Two lamellae for transmission electron microscopy were prepared by focused ion beam (FIB) using a Quanta 200 3D system. One lamella was cut in the longitudinal direction of the tape and the other one was cut in the transverse direction by analogy to the bridge configurations shown in figure 1(a). The microstructure of the samples was studied by transmission electron microscopy (TEM) using a TECNAI F20 field emission microscope at an accelerating voltage of 200 kV. The instrument was operated in HRTEM (high-resolution transmission electron microscopy) mode for lattice fringe imaging as well as in STEM (scanning transmission electron microscopy) mode under annular bright field conditions using a high-angle annular dark field detector (HAADF). The elemental composition was assessed by energy dispersive x-ray analysis using a EDAX SDD detector attached to the TEM.

3. Results and discussion

3.1. Transmission electron microscopy

Figure 2 shows low magnification annular bright field (ABF) images of the lamellae cut along the transverse (figure 2(a)) and longitudinal (figure 2(b)) directions. The

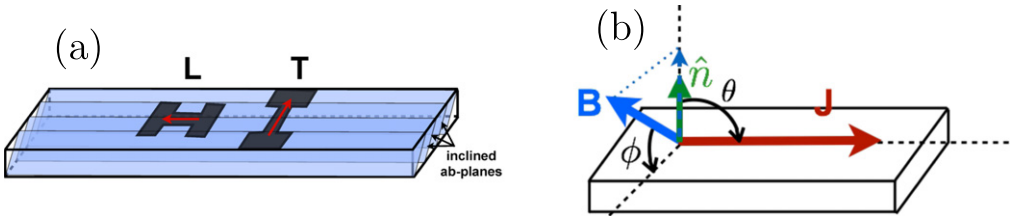

Figure 1. (a) Schematic diagram of the two bridge configurations, L-bridge and T-bridge, patterned on the tape. The red arrows show the current direction. (b) Schematic diagram of the two-axis rotation showing ϕ and θ. The unit vector $\hat{n}$ corresponds to the direction perpendicular to the tape surface.

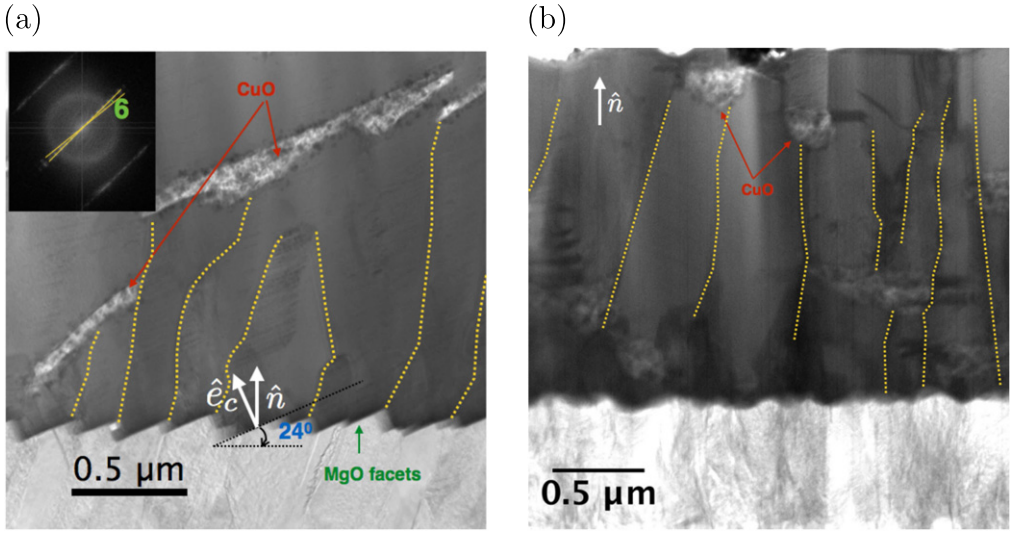

Figure 2. Annular bright field image of the (a) transverse lamella and (b) longitudinal lamella. Large CuO precipitates are present and the dashed yellow lines indicate the grain boundaries. The inset in (a) is a diffractogram obtained from an HRTEM image of a grain boundary showing a small misorientation of the two neighboring grains of about 6°.

grain boundaries in the GdBCO layer of the transverse lamella are tilted and meandering. They start at the edges of the MgO facets as shown by the dashed yellow lines in figure 2(a). The size of the grains varies from 200 nm to 900 nm. The grain boundary misorientation angles are small as shown by the diffractogram in the inset of figure 2(a). These inclined and meandering GBs are a characteristic of ISD-CCs and were also found in the DyBCO tapes grown by the same technique [4]. The GBs in the longitudinal lamella are planar and normal on average as shown in figure 2(b). The *c*-axis of the GdBCO was confirmed by HRTEM to be oriented parallel to the *c*-axis of the MgO buffer layer. The facet of the MgO buffer layer parallel to its (002) plane was found to be tilted by about 24° with respect to the plane of the tape. Thus, the *ab*-plane of the GdBCO layer was tilted by about 24° as well. A high density of stacking faults, which were characterized by double CuO chain intergrowths, was also found in the HRTEM images of the sample. They are indicated by the arrows in figure 3(b). Large CuO precipitates were observed in the GdBCO layer of both lamellae. The composition of these precipitates was confirmed by EDX. They are roughly cylindrical with their axis perpendicular to the tape direction and tilted by about 10–20° from the *ab*-planes (figure 2(a) and (b)).

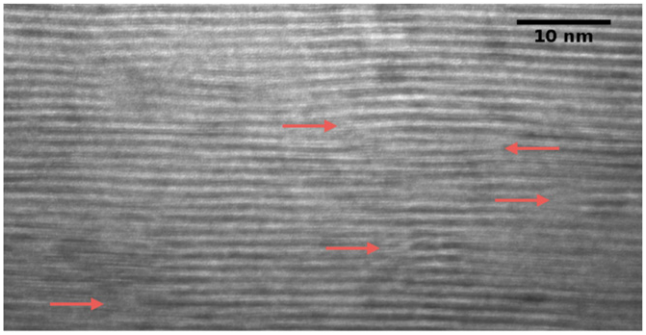

Figure 3. (a) HRTEM image of the transverse lamella. The stacking faults are indicated by the red arrows.

3.2. Transport measurement

3.2.1. Angular dependence of J_c in longitudinal current direction. The self-field J_c of the L-bridge at 77 K was 1.3 MA cm^{-2}. When the sample was rotated about the angle ϕ at the MLF configuration, the tilted crystallographic orientation of the GdBCO layer led to a peak at $\phi = 66°$ as shown in figure 4. This peak corresponds to the intrinsic pinning by the tilted *ab*-planes and an additional pinning contribution from the stacking faults parallel to the *ab*-planes. The presence of the $\hat{n}$-peak in the direction normal to the tape

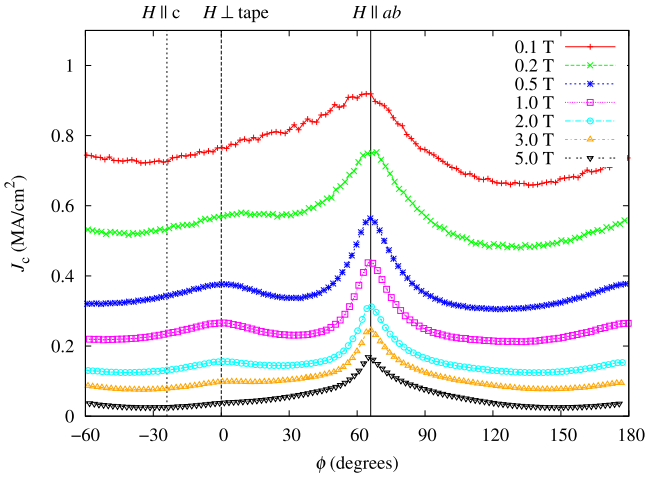

Figure 4. (a) $J_c(\phi)$ at $T = 77$ K and different applied fields for the L-bridge at maximum Lorentz force (MLF).

surface was induced by growth-related defects parallel to this direction. This smaller peak decreased as the field was increased.

For magnetic fields of 0.5 T and below, a slight shift in the *ab*-peak occurred as shown in figure 5(a). Upon reversing the direction of the applied field, which effectively reverses the direction of the Lorentz force acting on a vortex line, a difference in height of the *ab*-peak was seen and the *ab*-peak became highly asymmetric which led to a periodicity of the J_c anisotropy of 360° instead of the usual 180°-periodicity for tapes grown with the *ab*-planes parallel to the tape surface. Note that the two curves at different field orientations cross each other when the field is parallel to the *ab*-planes. The component of the Lorentz force which is parallel to the *ab*-plane and therefore moves the pancake vortices changes sign at this orientation. The pancake vortices enter the superconductor either from the interface with the substrate or from the opposite surface. The effect can thus be attributed to the difference in the surface roughness between the substrate–superconductor interface and superconductor surface which leads to different surface barriers for flux entry through the two interfaces. Note that this ISD sample has faceted MgO steps at the MgO–GdBCO interface that may cause this difference.

Another interesting property of the J_c-anisotropy was observed at high fields, namely the persisting asymmetry of the *ab*-peak down to 20 K as shown for 5 T in figure 5(b). The surface barrier effect should no longer be effective at high fields [8, 18] and it is worth noting that the high field curves (above 1 T) were reproducible upon reversal of the field or rotation, and thus the observed broken symmetry is not caused by hysteresis. Due to the tilt of the crystallographic axes of this tape and the additional presence of the inclined and meandering GBs, the rotation around the longitudinal axis can be classified into two angular regions. The first region occurs at $20° < \phi < 66°$ where the angle between the magnetic field and the average inclination of the GBs is comparatively small (shaded by red in figure 5(b)). On the other hand, in the second region, within $66° < \phi < 110°$ (shaded by violet), the angle between the applied field and the inclined GBs is larger (right inset in figure 5). The value of J_c in the first (red) region was observed to be lower than in the second (violet) one, which is quite unexpected regarding the present GBs because correlated defects often lead to a local maximum when the magnetic field is parallel and the Lorentz force is perpendicular to them (as in the present case). A direct limitation of the currents by the tilted grain boundaries is unlikely because the current flows parallel and does not have to cross them. (In this geometry, the current crosses the grain boundaries which are on average perpendicular to the tape.) We therefore conclude that the meandering grain boundaries in this case either do not significantly contribute to pinning, or contribute more efficiently if the vortices cross them, which is rather unlikely since the Lorentz force is parallel to the boundaries in that case. Another scenario that can be considered for the asymmetry around the *ab*-peak in the L-bridge is the effect of the vortex length which is larger in the violet region. However, the mechanism leading to the asymmetry in J_c remains to be clarified.

3.2.2. Angular dependence of J_c in transverse current direction. The self-field J_c of the T-bridge at 77 K was 0.88 MA cm^{-2}, which is 30% lower than the self-field J_c of the L-bridge. This was expected since the current has to cross the weakly superconducting planes [19]. The J_c-anisotropy of the T-bridge at the MLF configuration is shown in figure 6. The $\hat{n}$-peak was also found and was consistent with the behavior observed in the L-bridge (figure 6(a)). A minimum was observed at $H \| ab$ ($\phi = 90°$) that suppressed the formation of a peak resulting from intrinsic pinning. The minimum is a manifestation of vortex channeling. If the vortices in this angular regime are in a kinked state, the component of the Lorentz force parallel to the *ab*-plane, $F_{L\|ab}$, serves as the driving force that induces motion of the vortex strings and results in a decrease in J_c (see the schematic diagram in the inset of figure 6(a)). In contrast to the results on vicinal films [11] with no observable vortex channeling minimum at vicinal angles above 10° and on tilted IBAD-MgO tapes with tilt angles of 4–10° [9], a channeling minimum was observed in this tape up to temperatures as high as 77 K. Since the tilt of the crystallographic axes of GdBCO in this CC is more than twice as large as those reported in vicinal films, the component of the Lorentz force parallel to the *ab*-planes, $F_{L,\|ab}$, is also larger and is enough to overcome the suppression due to defects and shear forces. At 80 K, a very small trace of vortex channeling was observed and it disappeared at higher temperatures (figure 6(a)). This result agrees with the idea that a rectilinear vortex state persists above a certain temperature T_{cr} with a reported value of 80 K for YBCO [12, 20].

In view of the applications of coated conductors, it is also interesting to investigate the J_c-anisotropy in VLF-configuration since a large J_c may be achieved if the force-free (FF) geometry could be realized. The FF orientation is characterized by an effective zero Lorentz force by having parallel $\vec{B}$ and macroscopic $\vec{J}$ [21]. The most common VLF

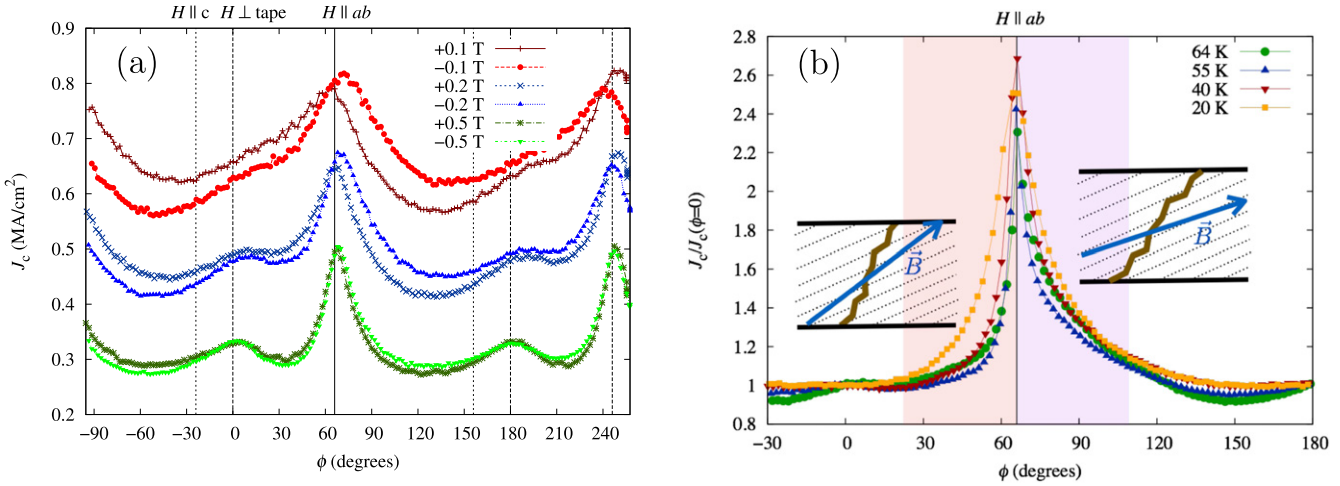

Figure 5. (a) $J_c(\phi)$ at 77 K and low fields. The influence of field reversal is also demonstrated. (b) $J_c(\phi)$ at 5 T and different temperatures. Two angular regions are shaded. The red region corresponds to the range in ϕ where the angle between the applied field and GBs is small (left inset) and J_c is lower. The angle between the applied field and GBs is larger in the violet region (right inset) with higher J_c.

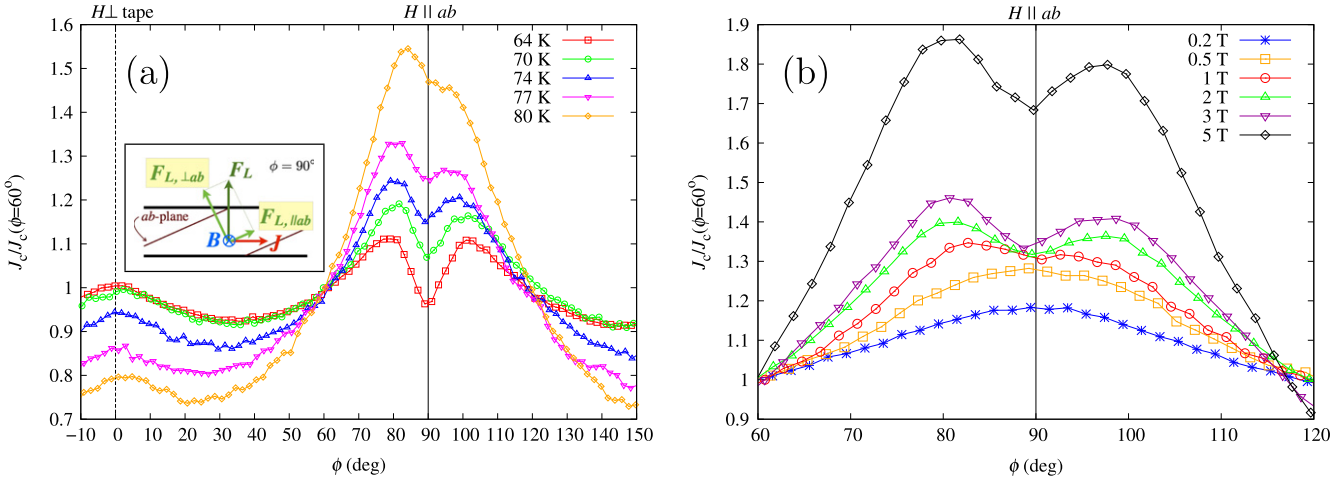

Figure 6. (a) Normalized $J_c(\phi)$ at $\mu_0 H_{\rm app} = 2$ T and different temperatures for the T-bridge in MLF configuration. The inset shows the Lorentz force vector acting on the vortex string when $\vec{B} \| ab$-planes ($\phi = 90°$). (b) Normalized $J_c(\phi)$ at $T = 77$ K and different applied fields.

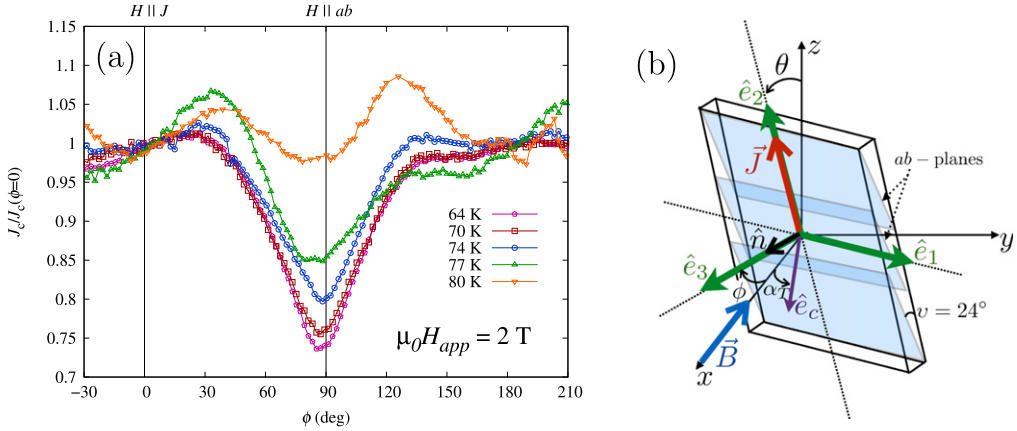

Figure 7. Normalized in-plane $J_c(\phi)$ of the T-bridge at different temperatures and $\mu_0 H_{\rm app} = 2$ T. (b) Geometry of the T-bridge in VLF configuration showing the sample unit vectors $\hat{e}_1$, $\hat{e}_2$ and $\hat{e}_3$ and the unit vector $\hat{e}_c$ parallel to the c-axis in the T-bridge.

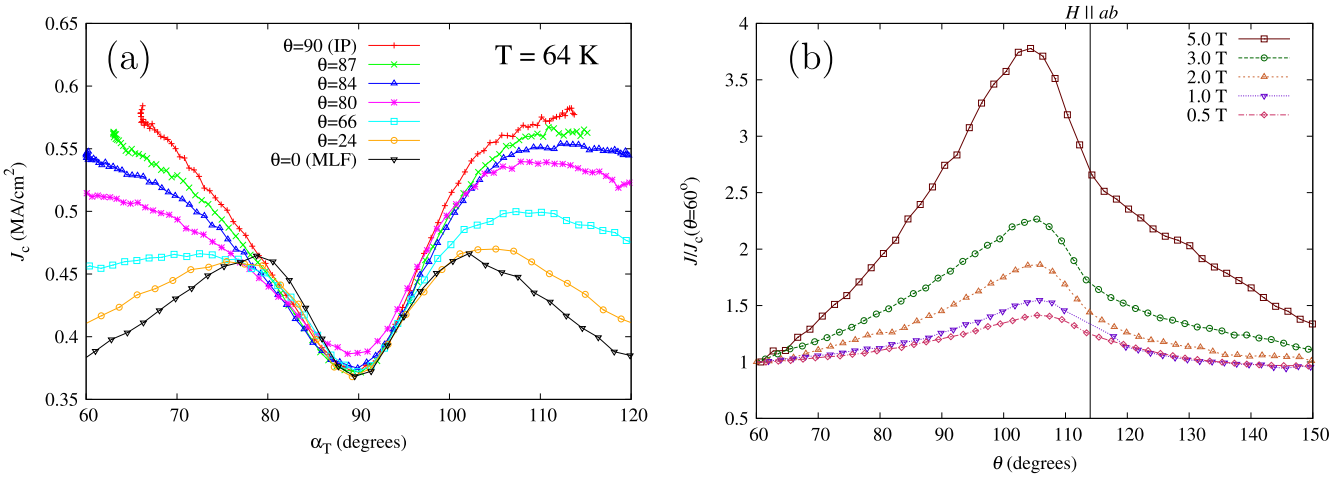

Figure 8. $J_c(\alpha)$ at different θ, $\mu_0 H_{app} = 5$ T and $T = 64$ K. (b) Normalized $J_c(\theta)$ of the T-bridge at 77 K and at different applied fields.

investigation is the in-plane (IP) measurement where the applied field is maintained parallel to the tape over the entire angular scan about ϕ at $\theta = 90°$. The results at 2 T and various temperatures are shown in figure 7(a). The vortex channeling minimum was again observed around $\phi = 90°$ at temperatures of 80 K and below for the same reason as in the MLF configuration. Interestingly, the FF peak which was expected at $\phi = 0$ was not apparent. For conventional coated conductors grown with the *ab*-planes parallel to the tape surface, a FF peak occurs when the applied field is oriented parallel to the macroscopic direction of current flow resulting in nearly zero Lorentz force [22]. For this ISD sample, the absence of an actual peak due to the FF configuration is a consequence of the tilted crystallographic axes of the sample. To further illustrate this, we consider the angle between the *c*-axis and the applied field denoted as α_T as shown in figure 7(b). The expression for α_T can be derived from the parametrization of three sample unit vectors $\hat{e}_1$,$\hat{e}_2$ and $\hat{e}_3$ (figure 7(b)), by rotations on ϕ and θ about the fixed *xyz*-coordinate of the sample space as done by Mishev *et al* [23].

$$\hat{e}_1 = \begin{pmatrix} -\sin\phi \\ \cos\phi \\ 0 \end{pmatrix} \hat{e}_2 = \begin{pmatrix} \cos\phi\sin\theta \\ \sin\phi\sin\theta \\ \cos\theta \end{pmatrix} \hat{e}_3 = \begin{pmatrix} \cos\phi\cos\theta \\ \sin\phi\cos\theta \\ -\sin\theta \end{pmatrix} \quad (1)$$

The direction of the magnetic field was fixed along the *x*-direction. For samples with tilted crystallographic axes and geometry as shown in figure 7(b), the angle α_T can be generally expressed as:

$$\alpha_T = \cos^{-1}[\cos\phi\cos(\upsilon - \theta)] \quad (2)$$

where υ is the tilt angle of the crystallographic axes and is equal to 24° in this study.

Figure 8(a) shows the plot of $J_c(\alpha_T)$ at various θ for 64 K and 5 T. This plot further illustrates that the apparent absence of the FF peak in figure 7(a) is actually an effect of the J_c anisotropy in the IP rotation and the maximum at $\alpha_T = 66°$ and $\alpha_T = 114°$ both corresponds to the FF orientation for $\theta = 90°$, where $\vec{J} \| \vec{B}$. At lower values of θ where the MLF configuration is approached, the large anisotropy between $H\|ab$ and $H\|c$ prevails, which would lead to an intrinsic peak that would be suppressed by the vortex channeling minimum (figure 6). The J_c curves at various θ converge within the angular range of α from 80° to 95°. The reasonable scaling of the J_c values in this angular range implies that the vortex channeling minimum is, as expected, independent of the out-of-plane component of the Lorentz force, $F_{L\perp ab}$, which changes with θ [23] and is only limited by the parallel component, $F_{L\|ab}$, which is independent of θ at fixed α_T.

Another VLF configuration in which the FF orientation can be achieved was established by an angular scan of θ at fixed ϕ. A data set at $\phi = 0$, $T = 77$ K and different fields is shown in figure 8(b). The rapid decrease of J_c before the kink at $\theta = 114°$ is a manifestation of vortex channeling which was found to be best visible at 5 T and which decreased in prominence at lower fields. Again, vortex channeling suppressed the *ab*-peak expected at $\theta = 114°$. Thus at 5 T, a peak at $\theta = 105°$ was visible and shifted to higher θ as the kink disappeared at lower fields. In contrast to vicinal YBCO films [11] where a sharp minimum is visible, vortex channeling manifests only as a kink in our data. The vortex channeling minimum is smeared out in our samples by the grain-to-grain misalignment of the *ab*-planes. The same indication of vortex channeling suppression was also reported in MOCVD/IBAD tapes with meandering GBs [13]. The FF peak expected at $\theta = 90°$ was again dominated by the anisotropy between the $H\|ab$ and $H\|c$ and thus a smooth decrease was observed in the data around $\theta = 90°$ where the FF configuration is expected.

3.2.3. Comparison of the anisotropy of the two current directions. The angle-resolved J_c of the L-and T-bridges is shown in figure 9(a). Both were plotted as a function of the angle between the *c*-axis and the applied field to allow a better comparison. The expression for α_T of the T-bridge is given by equation (1) and α_L for the L-bridge can be derived similarly as in section 3.2.1 It must be considered in the L-bridge configuration that $\hat{e}_c$ now lies in the $\hat{e}_1\hat{e}_3$-plane (figure 9(b)).

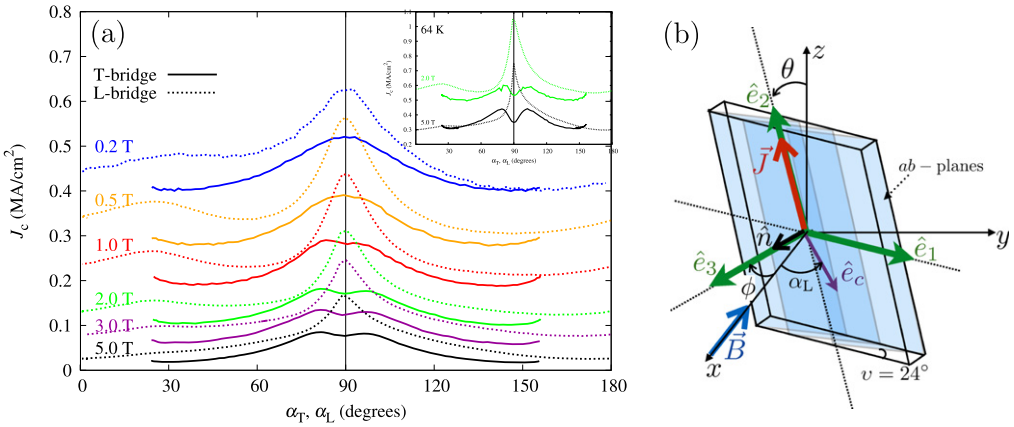

Figure 9. (a) Comparison of the J_c-anisotropy of the L- and T-bridge in MLF configuration at $T = 77$ K. J_c is shown as a function of the angle between the c-axis and the applied field to eliminate the effect of the crystallographic orientation with respect to the applied field. The inset shows $J_c(\alpha)$ at $T = 64$ K. (b) Geometry of the L-bridge in VLF configuration. In this arrangement, the vector $\hat{e}_c$ denoting the direction of the c-axis lies in the $\hat{e}_1\hat{e}_3$-plane.

The expression of α_L as a function of ϕ and θ is given by:

$$\alpha_L = \cos^{-1}(\cos\upsilon\cos\phi\cos\theta + \sin\upsilon\sin\phi). \quad (3)$$

As shown in figure 9(a), J_c at 77 K was consistently smaller in the T-bridge than in the L-bridge for the whole angular range. This is again what one can expect when the microscopic current flows across the weakly superconducting planes of GdBCO as mentioned in section 3.2.2 [19]. The difference between the J_c of the two bridges is largest at $H\|ab$ when vortex channeling decreased the J_c of the T-bridge to almost half the value of the L-bridge. Although J_c is smaller in the T-bridge, it is less anisotropic and the angular dependence is more symmetric around the *ab*-planes. At 64 K, the J_c difference between the two bridges was even smaller and, for small angular range, the J_c of the T-bridge exceeds that of the L-bridge at 5 T (inset of figure 9(a)) due to the asymmetric behavior in the L-bridge.

4. Summary

Angle-resolved measurements of the critical current density in a GdBCO-coated conductor deposited on ISD–MgO-buffered templates revealed an interesting anisotropic behavior both in the longitudinal and transverse current directions. The $J_c(\phi)$ curves in the longitudinal direction showed broken symmetry around the *ab*-peak. At lower fields, the asymmetry was influenced by different surface textures at the GdBCO surface and the faceted GdBCO–MgO interface. At higher fields, the mechanism of the $J_c(\phi)$-asymmetry remains to be clarified and the inclined and meandering GBs were not found to enhance pinning even if their orientation was parallel to the applied field.

Vortex channeling, which is characterized by a suppression of the *ab*-peak and appears as a minimum in angle-resolved J_c, was found in the transverse current direction at temperatures as high as 77 K. It was observed to be field dependent. Its occurrence at 77 K and high fields, which has not been reported so far, is a consequence of the large tilt of the crystallographic axes of the deposited superconducting layer by this ISD technique. The appearance of the channeling minimum makes J_c less anisotropic in the T-bridge than in the L-bridge. The competing effect of the Lorentz force and the crystallographic anisotropy of GdBCO on J_c at VLF is prominent in this CC due to its large crystallographic tilt and leads to an absence of an actual peak in the force-free orientation. The suppression of a vortex channeling minimum at lower fields and at the VLF configuration may also be a consequence of this competing effect in addition to the grain-to-grain misorientation of the *ab*-planes.

Acknowledgments

The authors would like to acknowledge Alexander Meledin for helpful discussions about the TEM results and Simon Lechner for the transport measurements provided for this paper. This work was supported by EUROTAPES which has received funding from the European Union Seventh Framework Programme [FP7/2-7-2013] under grant agreement no. NMP-LA-2012-280432.

References

[1] Foltyn S R, Civale L, MacManus-Driscoll J L, Jia Q X, Maiorov B, Wang H and Maley M 2007 *Nat. Mater.* **6** 631–42
[2] Pahlke P, Hering M, Sieger M, Lao M, Eisterer M, Usoskin A, Stroemer J, Holzapfel B, Schultz L and Huehne R 2015 *IEEE Trans. Appl. Supercond.* **25** 6603804
[3] Matsushita T, Kiuchi M, Kimura K, Miyata S, Ibi A, Muroga T, Yamada Y and Shiohara Y 2005 *Supercond. Sci. Technol.* **18** 227–31
[4] Duerrschnabel M, Aabdin Z, Bauer M, Semerad R, Prusseit W and Eibl O 2012 *Supercond. Sci. Technol.* **25** 105007
[5] Aabdin Z, Duerrschnabel M, Bauer M, Semerad R, Prusseit W and Eibl O 2012 *Acta Mater.* **25** 6592–600

[6] Matsumoto K and Mele P 2010 *Supercond. Sci. Technol.* **23** 014001
[7] Tachiki M and Takahashi S 1992 *Cryogenics* **32** 923–9
[8] Harrington S A, MacManus-Driscoll J L and Durrell J H 2009 *Appl. Phys. Lett.* **95** 022518
[9] Maiorov B, Gibbons B J, Kreiskott S, Matias V, Holesinger T G and Civale L 2005 *Appl. Phys. Lett.* **86** 132504
[10] Blatter G, Feigel'man M V, Geshkenbein V B, Larkin A I and Vinokur V M 1994 *Rev. Mod. Phys.* **66** 1125–388
[11] Durrell J H, Burnell G, Tsaneva V N, Barber Z H, Blamire M G and Evetts J E 2004 *Phys. Rev.* B **70** 214508
[12] Berghuis P, Bartolomeo E D, Wagner G A and Evetts J E 1997 *Phys. Rev. Lett.* **79** 2332–5
[13] Weigand M, Rutter N A, Sahonta S L and Durrell J H 2011 *IEEE Trans. Appl. Supercond.* **21** 3347–51
[14] Durrell J H, Hogg M J, Kahlmann F, Barber Z H, Blamire M G and Evetts J E 2003 *Phys. Rev. Lett.* **90** 247006
[15] Hogg M J, Kahlmann F, Tarte E J, Barber Z H and Evetts J E 2001 *Appl. Phys. Lett.* **78** 1433–5
[16] Palau A, Durrell J H, Macmanus-Driscoll J L, Harrington S, Puig T, Sandiumenge F, Obradors X and Blamire M G 2006 *Phys. Rev. Lett.* **97** 257002
[17] Prusseit W, Hoffman C, Nemetschek R, Sigl G, Handke J, Luemkemann A and Kinder H 2006 *IEEE Trans. Appl. Supercond.* **16** 996–8
[18] Bean C P and Livingston J D 1964 *Phys. Rev. Lett.* **12** 14–6
[19] Bauer M, Semerad R and Kinder H 1999 *IEEE Trans. Appl. Supercond.* **9** 1502–5
[20] Farrell D E, Rice J P, Ginsberg D M and Liu J Z 1990 *Phys. Rev. Lett.* **64** 1573–6
[21] Matsushita T, Kiuchi M and Otabe E S 2012 *Supercond. Sci. Technol.* **25** 125009
[22] Maiorov B *et al* 2007 *IEEE Trans. Appl. Supercond.* **17** 3697–700
[23] Mishev V, Seeboeck W, Eisterer M, Iida K, Kurth F, Haenisch J, Reich E and Holzapfel B 2013 *Appl. Phys. Lett.* **103** 232601